

Energy Gaps in Etched Graphene Nanoribbons

C. Stampfer, J. Güttinger, S. Hellmüller, F. Molitor, K. Ensslin, and T. Ihn

Solid State Physics Laboratory, ETH Zurich, 8093 Zurich, Switzerland

(Received 5 November 2008; published 3 February 2009)

Transport measurements on an etched graphene nanoribbon are presented. It is shown that two distinct voltage scales can be experimentally extracted that characterize the parameter region of suppressed conductance at low charge density in the ribbon. One of them is related to the charging energy of localized states, the other to the strength of the disorder potential. The lever arms of gates vary by up to 30% for different localized states which must therefore be spread in position along the ribbon. A single-electron transistor is used to prove the addition of individual electrons to the localized states. In our sample the characteristic charging energy is of the order of 10 meV, the characteristic strength of the disorder potential of the order of 100 meV.

DOI: 10.1103/PhysRevLett.102.056403

PACS numbers: 71.10.Pm, 73.21.-b, 81.05.Uw, 81.07.Ta

Graphene nanoribbons [1–8] display unique electronic properties based on truly two-dimensional (2D) graphene [9] with potential applications in nanoelectronics [10,11]. Quasi-1D graphene nanoribbons are of interest due to the presence of an effective energy gap, overcoming the gapless band structure of graphene and leading to overall semiconducting behavior, most promising for the fabrication of graphene transistors [5], tunnel barriers, and quantum dots [6–8]. Zone-folding approximations [12], π -orbital tight-binding models [13,14], and first principle calculations [15,16] predict an energy gap E_g scaling as $E_g = \alpha/W$ with the nanoribbon width W , where α ranges between 0.2–1.5 eV nm, depending on the model and the crystallographic orientation [4]. These theoretical estimates can neither explain the experimentally observed energy gaps of etched nanoribbons of widths beyond 20 nm, which turn out to be larger than predicted, nor do they explain the large number of resonances found inside the gap [1,2,8]. This has led to the suggestion that localized states due to edge roughness, bond contractions at the edges [16] and disorder may dominate the transport gap. Several mechanisms have been proposed to describe the observed gap, including renormalized lateral confinement [2], quasi-1D Anderson localization [17], percolation models [18] and many-body effects (including quantum dots) [19], where substantial edge disorder is required. Moderate amounts of edge roughness can substantially suppress the linear conductance near the charge neutrality point [20], giving rise to localized states relevant for both single particle and many-body descriptions. Here we show experimental evidence that the transport gap in an etched graphene nanoribbon [see schematic in Fig. 1(a)] is primarily formed by local resonances and quantum dots along the ribbon. We employ lateral graphene gates to show that size and location of individual charged islands in the ribbon vary as a function of the Fermi energy. In addition, we use a graphene single-electron transistor (SET) to detect individual charging events inside the ribbon.

We focus on an all-graphene setup, as shown in Fig. 1(b), where a nanoribbon (highlighted by dashed lines) with $W \approx 45$ nm is placed at a distance of ≈ 60 nm from a graphene SET with an island diameter of ≈ 200 nm. The back gate (BG) allows us to tune the overall Fermi level and the lateral graphene gates [21], plunger gate (PG) and side gates (SG1 and SG2) are used to locally tune the potential of the ribbon and the SET. A detailed description of the sample fabrication is found in Refs. [6,21–23]. The same process has also been used to pattern graphene Hall bars with mobilities on the order of $5000 \text{ cm}^2 \text{ V}^{-1} \text{ s}^{-1}$ [21]. The device is measured in two-terminal geometry

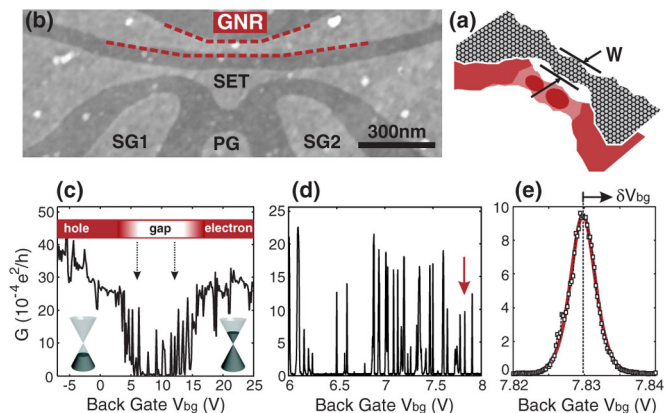


FIG. 1 (color online). (a) Schematic illustration of an etched nanoribbon with width W , highlighting local charge islands along the ribbon. (b) Scanning force microscope image of an etched graphene nanoribbon (GNR) with a nearby single-electron transistor (SET) and lateral gates (PG, SG1 and SG2). (c) Low bias ($V_b = 300 \mu\text{V}$) back-gate characteristics of the GNR showing that the regimes of hole and electron transport are separated by the transport gap, indicated by the vertical arrows. (d) High resolution close-up inside the gap displaying a large number of sharp resonances within the gap region. (e) Close-up of a single resonance [see arrow in panel (d)].

by low frequency lock-in techniques in a variable temperature insert cryostat at $T = 1.7$ K.

Figure 1(c) shows the low bias ($V_b = 300 \mu\text{V} \ll 4k_B T$) back-gate characteristic of the nanoribbon, where we tune transport from the hole (left-hand side) to the electron regime. The region $6 \text{ V} < V_{\text{bg}} < 12 \text{ V}$ of suppressed conductance (indicated by two arrows) is the so-called transport gap ΔV_{bg} in BG voltage ($\Delta V_{\text{bg}} \approx 6 \text{ V}$) [24]. In contrast to an energy gap predicted for samples without disorder, where transport is completely pinched-off, we observe—in good agreement with other experimental work [1,2,8]—a large number of reproducible conductance resonances inside the gap. A high-resolution close-up of Fig. 1(c) shown in Fig. 1(d) reveals a sequence of resonances with a small linewidth indicating strong localization. A particularly narrow resonance is shown in Fig. 1(e) [see arrow in Fig. 1(d)]. The line shape can be well fitted by $G \propto \cosh^{-2}(e\alpha_{\text{bg}}\delta V_{\text{bg}}/2.5k_B T_e)$, where $\alpha_{\text{bg}} \approx 0.2$ is the back-gate lever arm and $\delta V_{\text{bg}} = V_{\text{bg}} - V_{\text{bg}}^{\text{peak}}$ [26]. The estimated electron temperature, $T_e \approx 2.1$ K, is close to the base temperature, leading to the conclusion that the peak broadening is mainly limited by temperature rather than by the lifetime of the resonance. In Fig. 2(a) we show current measurements on the nanoribbon as a function of bias and BG voltage (i.e., Fermi energy). We observe regions of suppressed current leading to an effective energy gap in bias direction inside the transport gap in BG voltage [shown in Fig. 1(c)]. Highly nonlinear I - V characteristics [see, e.g., inset in Fig. 2(a)] are characteristic for the energy gap in bias direction. This energy gap agrees reasonably well with the observations in Refs. [2,19] of an energy gap of $E_g \approx 8 \text{ meV}$, for $W = 45 \text{ nm}$.

The transport gap in bias voltage corresponding to the energy gap E_g , and the transport gap ΔV_{bg} in back-gate voltage are two distinct voltage scales. The quantity ΔV_{bg} is measured at constant (nearly zero) V_b (transport window) but varying Fermi energy E_F and is related to a change in Fermi energy ΔE_F in the system. Varying the magnitude of the transport window V_b at fixed Fermi energy gives rise to E_g . We estimate the energy scale ΔE_F corresponding to ΔV_{bg} from $\Delta E_F \approx \hbar v_F \sqrt{2\pi C_g \Delta V_{\text{bg}} / |e|}$, where C_g is the back-gate capacitance per area [27]. We find an energy gap $\Delta E_F \approx 110\text{--}340 \text{ meV}$ which is more than 1 order of magnitude larger than E_g . We attribute this discrepancy to different physical meanings of these two energy scales.

More insight into the two energy scales is gained by focusing on a smaller BG voltage range as shown in Figs. 2(b) and 2(c) which are two high resolution differential conductance dI/dV_b close-ups of Fig. 2(a) (see labels therein). At this scale, transport is dominated by well distinguishable diamonds of suppressed conductance [see bright areas and dashed lines in Figs. 2(b) and 2(c)] which indicates that transport is blocked by localized electronic

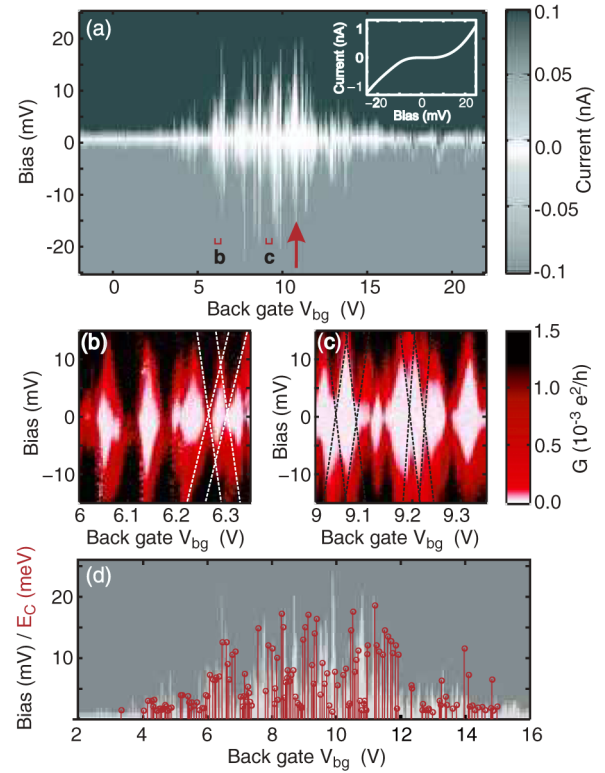


FIG. 2 (color online). (a) Current measurements as function of bias and back-gate voltage (all other gates are grounded) on the 45 nm wide nanoribbon [Fig. 1(a)]. The white areas are regions of strongly suppressed current forming the energy gap. The inset shows a typical nonlinear I - V characteristic ($V_{\text{bg}} = 10.63 \text{ V}$, see arrow). (b,c) Differential conductance (G) measurements as close-ups of panel (a) at two different back-gate regimes [see labels in (a)]. These measurements show diamonds with suppressed conductance (highlighted by dashed lines) allowing to extract the charging energy from individual diamonds. (d) Charging energies as function of the back-gate voltage over a wide range.

states or quantum dots (see also Ref. [25]). The charging energy E_c which itself is related to the quantum dot size, depends on the Fermi energy on a small BG voltage scale [see different diamond sizes in Figs. 2(b) and 2(c)], but also on a large scale [see Fig. 2(a)]. In order to confirm this statement the charging energies are plotted in Fig. 2(d) into the top half of the measurements shown in Fig. 2(a).

Figures 3(a) and 3(b) show conductance and differential conductance measurements at fixed BG as a function of the lateral PG voltage [cf. Fig. 1(b)] which tunes the potential on the nanoribbon locally. Similar to the BG dependent measurements in Fig. 1(d) we observe in Fig. 3(a) a large number of resonances inside the transport gap. In contrast to back-gate sweeps we find certain PG regions with almost equally spaced conductance peaks [see, e.g., the highlighted regime in Fig. 3(a) and the corresponding diamonds in Fig. 3(b)], giving rise to the assumption that here only a single charged island is tuned by the lateral

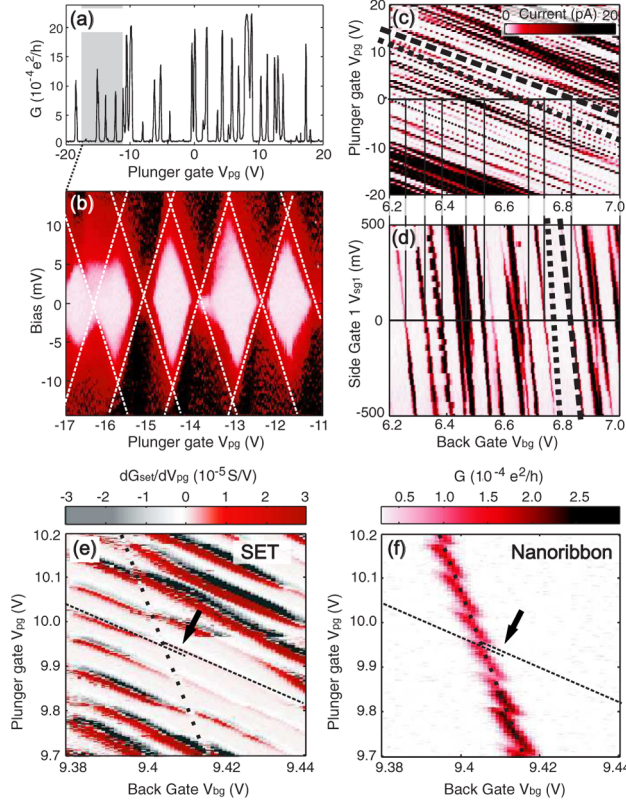


FIG. 3 (color online). (a) Low bias ($V_b = 300 \mu\text{V}$) conductance measurements as function of plunger gate voltage at fixed back gate ($V_{bg} = 7 \text{ V}$), showing a large number of sharp resonances within the gap region. (b) Corresponding diamonds [see highlighted area in panel (a)] in differential conductance G [same color scale as in Figs. 2(b) and 2(c)]. Here, a dc bias V_b with a small ac modulation ($50 \mu\text{V}$) is applied symmetrically across the ribbon. (c,d) Charge stability diagrams as function of plunger gate and back-gate voltage (c) and side gate 1 and back-gate voltage (d). These plots highlight that individual resonances have individual lever arms (see dashed and dotted lines). (e,f) Detection of individual charging events in the nanoribbon by the nearby SET. (e) Coulomb blockade resonances on the SET as function of V_{pg} and V_{bg} exhibit clear signatures of the charging event in the nanoribbon expressed by crossing the local resonance (f). Dotted and dashed lines show the different lever arms.

gate. These diamond measurements are of comparable quality as those presented in Refs. [6–8].

By following resonances at low bias ($V_b = 500 \mu\text{V}$) over a larger $V_{pg} - V_{bg}$ range [see Fig. 3(c)] we observe that individual resonances exhibit different relative lever arms in the range of $\alpha_{pg,bg} \approx 0.039\text{--}0.048$ [slopes of dotted and dashed lines in Fig. 3(c)]. These variations of up to 20% can be attributed to different capacitances between the PG and individual electron puddles, which sensitively includes their local position on the ribbon. By sweeping the voltage on the more asymmetrically placed SG1 [see Fig. 1(b)] rather than the PG this effect is even enhanced.

In Fig. 3(d) we show the corresponding measurements ($V_{pg} = 0 \text{ V}$). Relative lever arms in the range of $\alpha_{sg1,bg} \approx 0.054\text{--}0.077$ with scattering of more than 30% can be extracted. The stability of the sample allows to match resonances seen in Figs. 3(c) and 3(d) so that they can be followed in a 3D parameter space. These measurements confirm local resonances being located along the ribbon, with different lever arms to the local lateral gates.

We now make use of the SET device fabricated near the ribbon to detect individual charging events inside localized states of the nanoribbon. The SET which has been characterized before [28], has a charging energy of $E_{c,SET} \approx 4.5 \text{ meV}$ and Coulomb blockade peak spacing fluctuations below 15%. The Coulomb resonances in the conductance of the SET, highlighted as dashed lines in Fig. 3(e), can be used to detect charging of a local resonance [dotted line in Fig. 3(e)] in the nanoribbon with individual electrons. We show conductance measurements as function of PG and BG voltage in order to identify resonances of the SET and the nanoribbon via their different relative lever arms [Figs. 3(e) and 3(f)]. Since the SET is much closer to the PG than the nanoribbon, the relative lever arm $\alpha_{pg,SET}/\alpha_{bg,SET} \approx 0.18$ seen as the slope of SET resonances in Fig. 3(e) [dashed lines in Figs. 3(e) and 3(f)] is significantly larger than the relative lever arm of a resonance in the nanoribbon $\alpha_{pg,bg} \approx 0.04$ shown in Fig. 3(f) [dotted lines in Figs. 3(e) and 3(f)]. The observation of a jump [arrow in Fig. 3(e)] in the Coulomb resonances of the SET when they cross the resonance in the ribbon is a clear signature of charging the localized state in the nanoribbon, which changes in a discontinuous way the potential on the SET island by capacitive coupling. This shows that we accumulate localized charges along the nanoribbon as function of the BG voltage.

The experimental data shown above provide strong indications that the two experimentally observed energy scales E_g and ΔE_F are related to charged islands or quantum dots forming spontaneously along the nanoribbon. This is supported by the observation (i) of Coulomb diamonds, which vary in size as function of E_F , (ii) of a strong variation of the lever arms of individual resonances, and (iii) of local charging of islands inside the ribbon.

Quantum dots along the nanoribbon can arise in the presence of a quantum confinement energy gap (ΔE_{con})

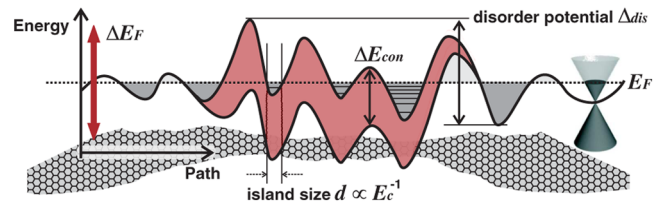


FIG. 4 (color online). Illustration of the potential landscape along the graphene nanoribbon allowing the formation of charged islands and quantum dots. For more details see text.

combined with a strong bulk and edge-induced disorder potential Δ_{dis} , as illustrated in Fig. 4. The confinement energy can be estimated by $\Delta E_{\text{con}}(W) \approx \gamma \pi a_{C-C}/W$, where $\gamma \approx 2.7$ eV and $a_{C-C} = 0.142$ nm [12]. This leads to $\Delta E_{\text{con}} = 26$ meV for $W = 45$ nm, which by itself can neither explain the observed energy scale ΔE_F , nor the formation of quantum dots in the nanoribbon. However, by superimposing a disorder potential giving rise to electron-hole puddles near the charge neutrality point [29], the confinement gap ensures that Klein tunneling (from puddle to puddle) gets substituted by real tunneling. Within this model ΔE_F depends on both the confinement energy gap and the disorder potential. An upper bound for the magnitude of the disorder potential can be estimated from our data to be given by ΔE_F . Comparing to Ref. [29] where a bulk carrier density fluctuation of the order of $\Delta n \approx \pm 2 \times 10^{11}$ cm $^{-2}$ was reported, we find reasonable agreement as the corresponding variation of the local potential is $\Delta E_F \approx \Delta E_{\text{con}} + \hbar v_F \sqrt{4\pi \Delta n} \approx 126$ meV.

We can estimate the fraction of overlapping diamonds by summing over all charging energies E_c observed in Fig. 2(d). This leads to $\sum E_c \approx 630$ meV. Comparison with the experimental estimate $\Delta E_F \approx 110$ –340 meV (see above) gives 45%–82% overlapping diamonds, strongly indicating statistical Coulomb blockade due to a number of quantum dots contributing to transport. We expect that the value of overlapping diamonds depends strongly on the length and the width of the nanoribbon in agreement with findings of Ref. [25].

The energy gap in bias direction E_g does not tell much about the magnitude of the disorder potential, but it is rather related to the sizes of the charged islands. In particular, the minimum island size is related to the maximum charging energy $E_{c,\text{max}}$, which defines E_g . By using a disc model we can estimate the effective charge island diameter by $d = e^2/(4\epsilon_0\epsilon E_c) \approx 100$ nm (where $\epsilon = (1 + 4)/2$), which exceeds the ribbon width W . Thus, in ribbons of different width the charging energy will scale with W giving the experimentally observed $1/W$ dependence of the energy gap in bias direction [2].

In conclusion, we have presented detailed transport measurements on a graphene nanoribbon, focusing on the origin of the transport gap. Experimentally we find two distinct energy scales characterizing this gap. The first is the charging energy of local resonances or quantum dots forming along the ribbon. The second is probably dominated by the strength of the disorder potential, but also depends on the gap induced by confinement due to the ribbon boundaries. These insights are important to understand transport in graphene nanostructures and may help in designing future graphene nanoelectronic devices.

During the preparation of this Letter we became aware of work on graphene nanoconstrictions reaching similar conclusions about the nature of the energy scales relevant for transport [30,31].

We thank A. Castro-Neto, S. Das Sarma, T. Heinzl, M. Hilke, F. Libisch, K. Todd and L. Vandersypen for helpful discussions. Support by the SNSF and NCCR are gratefully acknowledged.

-
- [1] Z. Chen *et al.*, Physica E (Amsterdam) **40**, 228 (2007).
 - [2] M. Y. Han *et al.*, Phys. Rev. Lett. **98**, 206805 (2007).
 - [3] X. Li, X. Wang, L. Zhang, S. Lee, and H. Dai, Science **319**, 1229 (2008).
 - [4] Y.-M. Lin *et al.*, Phys. Rev. B **78**, 161409R (2008).
 - [5] X. Wang, Y. Ouyang, X. Li, H. Wang, J. Guo, and H. Dai, Phys. Rev. Lett. **100**, 206803 (2008).
 - [6] C. Stampfer *et al.*, Appl. Phys. Lett. **92**, 012102 (2008).
 - [7] L. A. Ponomarenko *et al.*, Science **320**, 356 (2008).
 - [8] C. Stampfer *et al.*, Nano Lett. **8**, 2378 (2008).
 - [9] A. K. Geim and K. S. Novoselov, Nature Mater. **6**, 183 (2007).
 - [10] M. I. Katnelson, Mater. Today **10**, 20 (2007).
 - [11] B. Trauzettel *et al.*, Nature Phys. **3**, 192 (2007).
 - [12] C. T. White, J. Li, D. Gunlycke, and J. W. Mintmire, Nano Lett. **7**, 825 (2007).
 - [13] N. M. R. Peres, A. H. Castro Neto, and F. Guinea, Phys. Rev. B **73**, 195411 (2006).
 - [14] D. Dunlycke, D. A. Areshkin, and C. T. White, Appl. Phys. Lett. **90**, 142104 (2007).
 - [15] J. Fernandez-Rossier, J. J. Palacios, and L. Brey, Phys. Rev. B **75**, 205441 (2007).
 - [16] L. Yang, C.-H. Park, Y.-W. Son, M. L. Cohen, and S. G. Louie, Phys. Rev. Lett. **99**, 186801 (2007).
 - [17] E. R. Mucciolo *et al.*, arXiv:0806.3777v1 [Phys. Rev. B (to be published)].
 - [18] S. Adam, S. Cho, M. S. Fuhrer, and S. Das Sarma, Phys. Rev. Lett. **101**, 046404 (2008).
 - [19] F. Sols, F. Guinea, and A. H. Castro Neto, Phys. Rev. Lett. **99**, 166803 (2007).
 - [20] M. Evaldsson, I. V. Zozoulenko, Hengyi Xu, and T. Heinzl, Phys. Rev. B **78**, 161407(R) (2008).
 - [21] F. Molitor *et al.*, Phys. Rev. B **76**, 245426 (2007).
 - [22] K. S. Novoselov *et al.*, Science **306**, 666 (2004).
 - [23] D. Graf *et al.*, Nano Lett. **7**, 238 (2007).
 - [24] This is a rather rough approximation and the arrows in Fig. 1(c) are just pointing to the region of the gap. A more quantitative definition of ΔV_g is discussed in Ref. [25].
 - [25] F. Molitor *et al.*, arXiv:0811.0676.
 - [26] C. W. J. Beenakker, Phys. Rev. B **44**, 1646 (1991).
 - [27] We assume that the charge neutrality point is in the center of the transport gap ($V_{\text{bg}}^D \approx 9$ V) and we make use of the following boundary conditions for $C_g(W)$. Lower bound: $C_g(W \rightarrow \infty) = C_{g,2D} \approx 7.2 \times 10^{10}$ cm $^{-2}$ V $^{-1}$ |e|. Upper bound: Following Ref. [4] the ratio $C_g(W)/C_{g,2D}$ increases with decreasing W/d , where d is the oxide thickness, and we obtain $C_g(W = 30$ nm) $\approx 10 C_{g,2D}$.
 - [28] J. Güttinger *et al.*, Appl. Phys. Lett. **93**, 212102 (2008).
 - [29] J. Martin *et al.*, Nature Phys. **4**, 144 (2008).
 - [30] K. Todd *et al.*, Nano Lett. **9**, 416 (2009).
 - [31] X. Liu *et al.*, arXiv:0812.4038.